ChemPubSoc Europe

DOI: 10.1002/chem.201405068

CHEMISTRY
A European Journal
Full Paper

Porous Materials |Hot Paper|

Porous Carbon Anodes for a High Capacity Lithium-Ion Battery Obtained by Incorporating Silica into Benzoxazine During Polymerization

De-Cai Guo, Fei Han, and An-Hui Lu*[a]

Abstract: Porous carbon anodes with a controllable V_{mes}/V_{mic} ratio were synthesized through the self-assembly of poly(benzoxazine-co-resol) and the simultaneous hydrolysis of tetraethyl orthosilicate (TEOS) followed by carbonization and removal of silica. The V_{mes}/V_{mic} ratio of the carbon can be controlled in the range of approximately 1.3–32.6 through tuning the amount of TEOS. For lithium-ion battery anodes, a correlation between the electrochemical performance and V_{mes}/V_{mic} ratio has been established. A high V_{mes}/V_{mic} ratio in porous carbons is favorable for enhancing the accessibility of Li ions to active sites provided by the micropores and for achieving good lithium storage performance. The obtained porous carbon exhibits a high reversible capacity of 660 mAh g^{-1} after 70 cycles at a current density of 100 mA g^{-1}. Moreover, at a high current density of 3000 mA g^{-1}, the capacity still remains at 215 mAh g^{-1}, showing a fast charge-discharge potential. This synthesis method relying on modified benzoxazine chemistry with the hydrolysis of TEOS may provide a new route for the development of mesoporous carbon-based electrode materials.

Introduction

The increasing need of rechargeable power batteries in emerging electric vehicles and hybrid electric vehicles has spurred tremendous research effort in developing lithium-ion batteries (LIBs) with high reversible capacity and fast charge-discharge capability.[1–8] To date, graphite has been the most commonly used anode material in commercial LIBs. However, the low theoretical capacity of 372 mAh g^{-1} and poor rate performance induced by the low lithium solid-state diffusion coefficient of $10^{-7}\sim10^{-10}$ cm^2 s^{-1} have hindered the application of graphite in the rapidly developing LIB market.[9,10] In the search for advanced anode materials, porous carbons with a large number of Li-ion storage active sites and a loose skeleton structure (vs. graphite) are attracting much interest due to their high available capacity and negligible volumetric expansion. Recent research efforts have therefore been devoted to exploring nanostructured porous carbon anodes that possess a high energy density and reliable safety.[11–17] However, bulky and microporous carbons suffer from low lithium diffusion rate within their frameworks, thus limiting their rate capability.[18] Moreover, the active surfaces provided by micropores are difficult to fully utilize because of the sluggish Li-ion transport, thus resulting in a low reversible capacity.[19,20]

When considering the improvement of the capacity of porous carbon anodes, a short lithium diffusion path and a high electrode/electrolyte contact surface area should be the key factors. One of the effective solutions is to introduce mesopores into the porous carbon framework that allows rapid transport channels for solvated Li ions, reducing the time of Li-ion diffusion.[21–23] For example, a mesoporous hollow carbon anode with large surface area and mesopore volume delivers a very high reversible capacity of $\approx$1100 mAh g^{-1} at 100 mA g^{-1}.[24] When using a two-dimensional ordered mesoporous carbon nanosheet as an anode, a Li-ion storage capacity of 833 mAh g^{-1} at 100 mA g^{-1} was achieved.[25] Most work aimed at achieving a mesoporous structure can facilitate Li-ion diffusion to reach active sites and improve the utilization of the active surface area, thus achieving efficient Li-ion storage. However, a few studies have paid attention to the effect of the volume ratio between mesopores and micropores on the electrochemical properties of porous carbons.

In this work, we report a synthesis of porous carbons by mixing benzoxazine precursors and TEOS, followed by the simultaneous polymerization of the benzoxazine and hydrolysis of the TEOS, which are triggered by the addition of 1,6-diaminohexane (DAH), providing an alkaline environment. Hence, a homogeneous system can be obtained without any phase separation. The volume ratio of mesopores to micropores in the range of approximately 1.3–32.6 can be controlled by tuning the amount of TEOS used in the reaction system. The synthesized porous carbon used as an anode material of a lithium-ion battery presents a high reversible capacity of 660 mAh g^{-1} even after 70 cycles at a current density of 100 mA g^{-1}, and good rate performance. At a high current density of 3000 mA g^{-1}, the capacity still remains at 215 mA h g^{-1}.

[a] Dr. D.-C. Guo, Dr. F. Han, Prof. Dr. A.-H. Lu
State Key Laboratory of Fine Chemicals, School of Chemical Engineering, Dalian University of Technology, Dalian 116024 (P. R. China)
E-mail: anhuilu@dlut.edu.cn

Results and Discussion

Considering the advantage of the rapid polymerization of benzoxazine, we proposed a co-assembly route of poly(benzoxazine) and silica by tuning the reaction rate. In the reaction system, the DAH used acts not only as the precursor of benzoxazine but also as a basic catalyst for facilitating the hydrolysis of TEOS. By varying the amount of TEOS, a series of samples were prepared. All the samples were derived from a homogeneous emulsion. After the aging and subsequent carbonization, and the removal of silica, porous carbon was produced.

The morphologies of porous carbon were observed by scanning electron microscopy (SEM). As shown in Figure 1, the porous carbons have a continuous skeleton structure decorated with carbon spheres. The diameter of the carbon spheres is approximately 200–300 nm (Figure 1a, b). A further increase in the amount of TEOS used leads to a decrease of the diameter of the carbon spheres (Figure 1c). In the case of PC-80, no carbon spheres can be seen in the porous carbon framework.

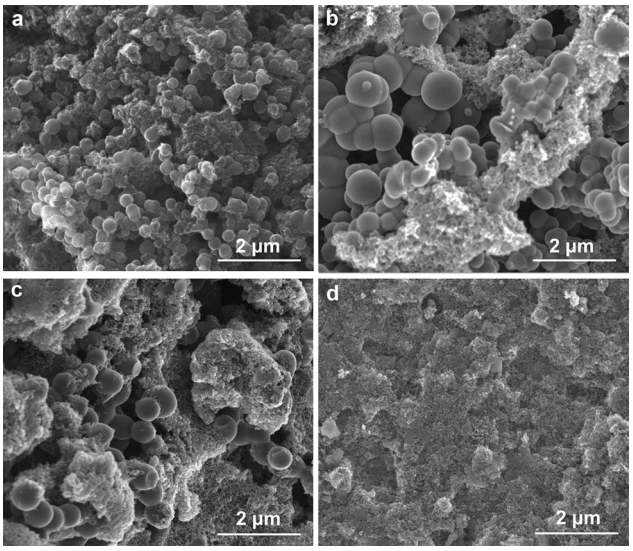

Figure 1. SEM images of a) PC-50, b) PC-60, c) PC-70, and d) PC-80.

The porous structures of the carbons were characterized by nitrogen sorption at 77.4 K. As seen from Figure 2a, all the isotherms have a typical type IV shape with a type H2 hysteresis located at a relative pressure of 0.4–0.95, indicating a predominantly mesoporous structure.[26] The specific surface areas increase from 855 $m^2 g^{-1}$ for PC-50 to the maximum value of 1110 $m^2 g^{-1}$ for PC-70, then decrease to 936 $m^2 g^{-1}$ for PC-80. The change of pore volumes of the four samples is similar to that of their specific surface areas (Table 1). Pore size distributions (PSDs) of all the samples in Figure 2b are concentrated at approximately 3–5 nm and 30 nm. To investigate the origin of these two kinds of mesopores, N_2 sorption measurements of two carbon-silica hybrids (CSHs: CSH-60 and CSH-70) were carried out to distinguish the porous structures. Moreover, one carbon sample (PC-0) was synthesized under the same conditions but without the addition of TEOS. The isotherms of CSH-60 and CSH-70 are of type IV with hysteresis at a relative pressure of 0.65–0.95 (Figure 2c) and the PSDs of CSH-60 and CSH-70 show a single peak located around 20–30 nm (Figure 2d). Compared with the smaller pores of 5.4 nm in PC-0 (Figure 2d), it is clear that the bigger pores of 20–30 nm in the CSHs and PCs are mainly derived from a cooperative assembly between the surfactant and the inorganic phase derived from TEOS.[27–30] For the bimodal pore size distribution in PC-60 and PC-70 (Figure 2b), the 3–5 nm pores were produced after the removal of silica from CSHs, which is similar to pore generation from the nanocasting method.[31] Meanwhile, the pristine pores at 20–30 nm still remained, suggesting the robustness of the porous carbon skeleton. Such a hierarchical porous structure offers more active sites for the insertion and storage of lithium ions,[24] facilitates effective strain accommodation during bulk volume expansion-contraction, and improves the accessibility of the active sites to lithium ions.[32]

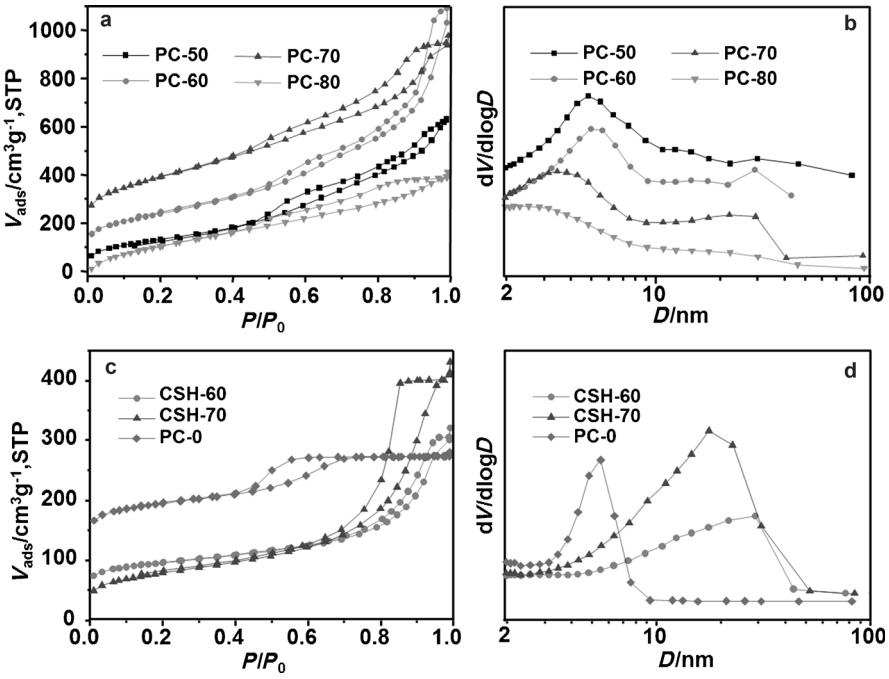

Figure 2. a,c) N_2 sorption isotherms, and b,d) the corresponding PSDs of the porous carbons and carbon-silica hybrids. The isotherms of PC-50, PC-70, and PC-80 were offset vertically by 80, 80, and 160 $cm^3 g^{-1}$ STP, respectively.

Table 1. Structural parameters[a] and electrochemical properties of porous carbons and their carbon-silica hybrids.

Sample	C:SiO_2 weight ratio	S_{BET} [$m^2 g^{-1}$]	D_{peak} [nm]	V_{total} [$cm^3 g^{-1}$]	V_{mic} [$cm^3 g^{-1}$]	V_{mes}/V_{mic}	initial reversible capacity
PC-0	100:0	670	5	0.46	0.2	1.3	337
PC-50	52:48	876	4.8, 28	1.16	0.15	6.7	514
PC-60	40:60	855	5, 28	1.68	0.05	32.6	717
PC-70	29:71	1110	3, 29	1.39	0.05	26.8	738
PC-80	19:81	936	3, 25	0.88	0.08	11	500
CSH-60	40:60	331	28	0.50	0.08	–	–
CSH-70	30:70	275	21	0.67	0.03	–	–

[a] S_{BET}: apparent surface area calculated from the adsorption data in the relative pressure range of 0.05 to 0.3 using the Brunauer–Emmett–Teller (BET) method; D_{peak}: determined from the adsorption branches of the isotherms using Barrett–Joyner–Halenda (BJH) model; V_{total}: total pore volume at $P/P_0 = 0.99$; V_{mic}: micropore volume calculated by t-plot method; V_{meso}: $V_{total} - V_{mic}$.

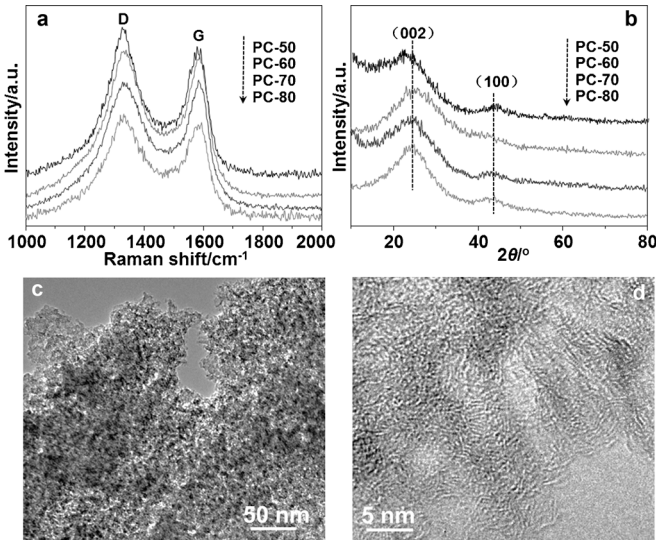

Figure 3. a) Raman spectra, and b) wide-angle powder XRD patterns of PC-50, PC-60, PC-70, and PC-80, c,d) TEM images of PC-60.

The graphitic structures of the samples were characterized by Raman spectroscopy. As shown in Figure 3a, the peaks observed at 1590 and 1350 cm^{-1} are attributed to the G (stretching mode of graphite) and D (breathing mode) bands, respectively. This indicates that the porous carbons have partially graphitized domains. The samples were also subjected to X-ray diffraction (XRD) analysis. As can been seen in Figure 3b, the peaks are identified as a typical (002) interlayer peak of graphitic carbon at $2\theta = 25^\circ$, indicating that graphitic structures are developed to a certain extent. The weak peak at 43° (the 100 diffraction peak for graphite) indicates the formation of a high degree of interlayer condensation and small crystal size of the carbon skeleton. The 100 diffraction peak shows a tail at the high-angle side, further indicative of the co-existence of local graphitization with turbostratic carbon materials. As seen from the TEM images of sample PC-60 (Figure 3c,d), the carbon skeleton contains abundant mesopore, micropore, and turbostratic structures. These results reveal that the reaction system of poly-benzoxazine and TEOS results in the formation of a continuous carbon skeleton and turbostratic graphitized domains.

To further understand the surface chemistry and the structural evolution of sample PC-60, infrared (IR) microspectroscopy and X-ray photoelectron spectroscopy (XPS) analyses were performed. As can be seen in Figure 4a, there are several characteristic peaks attributed to functional groups, such as C=C, C–H, C=O, and O–H.[33,34] The

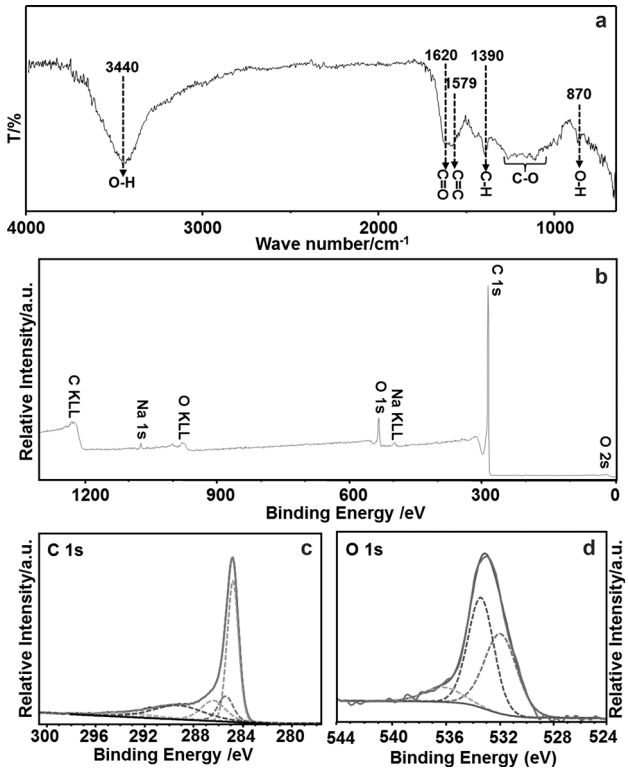

Figure 4. a) IR spectra, b) XPS spectra, c) the fitted C 1s spectrum, and d) O 1s spectrum of sample PC-60.

peaks around 1620 and 1580 cm^{-1} are attributed to the C=O and C=C stretching vibration, which shows the presence of aromatic rings. The peak at 1390 cm^{-1} is attributed to the out-of-plane deformation vibrations of C–H, and the peaks at 1200 to 1093 cm^{-1} are attributed to the C–O stretching vibration. From Figure 4b, the absence of the peak assigned to the Si–O stretching vibration confirms the removal of silica from the carbon–silica hybrid. The C and O species of PC-60 were further determined by XPS fine scanning (Figure 4c,d). As shown in the XPS C 1s spectrum (Figure 4c), the most pronounced peak located at 284.8 eV is characteristic of the carbon lattice, and the remaining peaks are –C–OH (285.5 eV), –C=O

(286.4 eV), –COOH (288.6 eV), and carbonate (291.2 eV) in sequence.[35,36] The O 1s spectrum indicates the presence of three types of oxygen bonds: –C=O (531.6 eV), –C–OH (533.6 eV), and –COOH (536.1 eV) (Figure 4d).[37–39]

Owing to the well-developed and controllable mesoporosity and good electrical conductivity of the porous carbons, they were evaluated as LIB anodes by a galvanostatic charge-discharge test in the voltage range from 0.005 to 3 V (Figure 5).

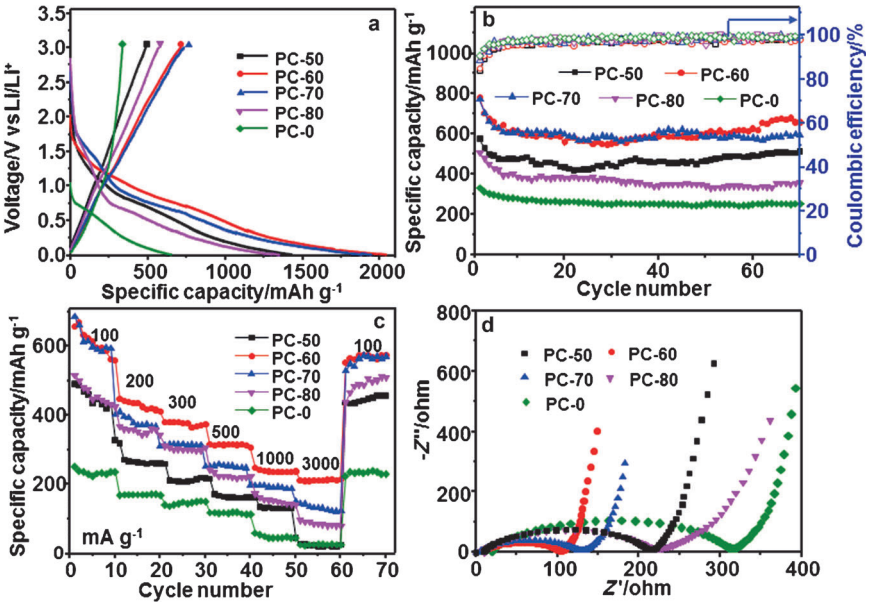

Figure 5. a) Galvanostatic charge-discharge curves at 100 mA g^{-1} for the porous carbon (the first cycle). b) Cycling performance and coulombic efficiency of the porous carbon. c) Rate performance of the porous carbon at different current densities from 100 to 3000 mA g^{-1} and then back to 100 mA g^{-1}. d) Typical Nyquist plots observed for different electrode materials.

For comparison, the electrochemical performance of PC-0 synthesized without using TEOS was also investigated. Figure 5a shows the first-cycle charge-discharge voltage profiles of these carbon anodes at a current density of 100 mA g^{-1}. They display similar electrochemical voltage behavior to that of previously reported porous carbon anodes.[11,25,41] Importantly, these carbon anodes show remarkably different specific capacities in the first cycle. Samples PC-0, PC-50, PC-60, PC-70, and PC-80 exhibit initial reversible capacities of 337, 515, 717, 738, and 500 mAh g^{-1} with coulombic efficiencies of 42, 34, 35, 38, and 41%, respectively. Obviously, PC-60 and PC-70 have higher capacities than their counterparts, and the values correspond to twice the theoretical capacity of graphite (i.e., 372 mAh g^{-1}). A large irreversible capacity is observed in the first discharge-charge process. The low initial coulombic efficiency is a well-accepted phenomenon in carbon nanostructures,[11,25,41] which is related to the high active surface area. Further work is in progress to reduce the first irreversible capacity on these interesting carbon nanomaterials by a pre-lithiation method.

The cycle stability during the Li insertion-extraction processes is an important factor in the use of carbon materials as anodes for lithium-ion batteries. Figure 5b shows the comparative cycle performance and coulombic efficiency of various carbon materials at 100 mA g^{-1}. It can be observed that the coulombic efficiencies of all carbon anodes increase dramatically with the increasing number of cycles, reaching over 98% after 10 cycles. The cycling performance of all carbon anodes was found to be relatively stable after 10 cycles. It should be pointed out that the cycle stability here is superior to those reported for mesoporous carbon anodes.[11,18,24] Compared with the other carbon materials in this study, PC-60 delivers the highest specific capacity of 660 mAh g^{-1} after 70 cycles. To the best of our knowledge, both the reversible capacity and cycle stability are superior to those of most previously reported porous carbon anodes for LIBs.[40,41] Cycled at the same current density, the reversible capacities of PC-50 (514 mAh g^{-1}), PC-70 (593 mAh g^{-1}) and PC-80 (359 mAh g^{-1}) are significantly lower than that of PC-60. In sharp contrast, the reversible capacity of PC-0 electrodes is only 255 mAh g^{-1}, which is even lower than the practical capacity of commercial graphite. In the cases of samples PC-50 and PC-80, because the former has bigger mesopore and micropore volumes, it has a higher reversible capacity. Samples PC-60 and PC-70 have similar mesopore and micropore volumes; therefore they have similar reversible capacities. These results indicate that carbon materials with well-developed mesoporous structures originating from the removal of silica exhibit a large Li storage capacity. The amount of TEOS used for the preparation of the porous carbon materials also has an impact on the reversible capacity, possibly due to the different V_{mes}/V_{mic} ratios. Previously, the Maier[18] and Yu groups[24] have demonstrated that a larger V_{mes}/V_{mic} ratio can effectively improve the utilization of pore channels in carbon materials, thus leading to a higher Li storage capacity and better rate capability. Therefore, the rate performance was also studied to better understand the importance of the V_{mes}/V_{mic} ratio. Figure 5c shows the variations of the reversible capacities of the carbon anodes at different current densities. The cells were first cycled at 100 mA g^{-1} for 10 cycles, followed by cycling at current densities increasing stepwise to as high as 3000 mA g^{-1}. Compared with the other carbon anodes, PC-60 has a superior rate performance. A specific charge capacity of around 380 mAh g^{-1} was obtained at 500 mA g^{-1}, 240 mA h g^{-1} at 2000 mA g^{-1}, and 215 mA h g^{-1} at 3000 mA g^{-1}. A constant capacity of 580 mAh g^{-1} was restored when the current density was reversed to 100 mA g^{-1} even after 70 cycles. Furthermore, the rate capability in this present work is strongly dependent on the V_{mes}/V_{mic} ratio of the carbon materials. A larger V_{mes}/V_{mic}

ratio means a better rate capability, which is due to faster mass transport of conductive ions to reach active sites and again confirms the importance of the V_{mes}/V_{mic} ratio.

To determine the relationship between the Li-ion storage performance and the pore structure of these porous carbons, EIS measurements were carried out to verify the kinetics of Li-ion insertion. Representative Nyquist plots are shown in Figure 5d for the five porous carbon anode materials. All the Nyquist plots are similar to each other in shape, consisting of one depressed semicircle at high/medium frequency and an inclined line at low frequency. In general, the intercepts on the real axis are considered as the total resistance of the electrolyte, separator, and electrical contacts.[41,42] The semicircle is ascribed to the sum of the contact resistance, the solid electrolyte interphase (SEI) resistance, and the charge-transfer resistance, whereas the inclined line at approximately 45° to the real axis corresponds to the lithium-diffusion process within a carbon electrode.[21,41] It is apparent that the PC-60 electrode with the largest V_{mes}/V_{mic} ratio shows the smallest semicircle diameter, followed in order by PC-70, PC-80, PC-50, and PC-0 with the smallest V_{mes}/V_{mic} ratio (Table 1). This reveals that the electrochemical reaction resistance increases in the order PC-60 < PC-70 < PC-80 < PC-50 < PC-0, indicating that PC-60 has the fastest Li-ion insertion kinetics.

From the aforementioned results, it seems that the two important performance parameters, namely initial reversible lithium-ion storage capacity and cycle stability, are strongly dependent on the pore structures (e.g., V_{mes}/V_{mic} ratio) of the carbon electrode materials. In summary, we propose the relationships between the (ir)reversible capacity and the pore structure that are shown in Figure 6. As can be seen, a good

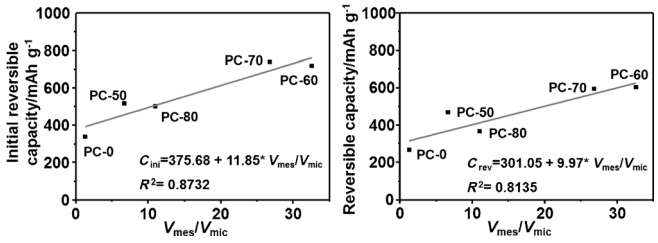

Figure 6. (a) The relationship between V_{mes}/V_{mic} and initial reversible capacity, (b) the relationship between V_{mes}/V_{mic} and the average reversible capacity from 6 to 50 cycles.

linear relationship between the initial discharge capacity (C_{ini}) and the V_{mes}/V_{mic} ratio can be obtained by plotting the experimental C_{ini} versus V_{mes}/V_{mic} (Figure 6a). It indicates that the large V_{mes}/V_{mic} ratio is favorable for enhancing the accessibility of Li ions to reach active sites provided by micropores. The good linear relationship between the average reversible capacity from 6 to 50 cycles (C_{rev}) and the V_{mes}/V_{mic} ratio also shows a similar correlation as mentioned above (Figure 6b). These results confirmed that mesopores in carbon anodes can provide rapid-transport channels for solvated Li ions and reduce the solid-state diffusion pathway for Li ions, effectively increasing the active surface of micropores and enhancing the utilization of micropores. Therefore, a high proportion of mesopores in a porous carbon anode would allow one to achieve good lithium storage performance.

Conclusion

In this study, porous carbons with a controllable V_{mes}/V_{mic} ratio have been synthesized, which show good lithium storage performance. The synthesis method is based on the organic–inorganic–surfactant co-assembly method using silica and poly-benzoxazine as building blocks, followed by the removal of silica. The key to the synthesis is to balance the kinetics of phase separation versus gelation of the silica induced by DAH matching the gelation/polymerization of benzoxazine. These materials demonstrate excellent performance in lithium-ion batteries. In particular, sample PC-60 has both a high reversible specific capacitance of 660 mAh g^{-1} at a current density of 100 mA g^{-1} and excellent long-term cycle stability. It also has an excellent rate performance even at a high current density of 3000 mA g^{-1}, where the reversible capacitance can reach 215 mA h g^{-1}. This study offers a new and easy synthesis method for porous carbons with a bimodal pore system, and also ensures wide applications of such materials in electrochemical energy storage.

Experimental Section

Chemicals

Resorcinol (denoted R, 99.5%) and formalin (37 wt%) were purchased from Tianjin Kermel Chemical Reagent Co., Ltd. 1,6-diaminohexane (DAH, 99.0%), ethanol (99.7%), and tetraethyl orthosilicate (TEOS, 99%) were all supplied by Sinopharm Chemical Reagent Co., Ltd. Pluronic F127 was purchased from Sigma–Aldrich. All chemicals were used as received.

Synthesis of porous carbons

The porous carbons were prepared through simultaneous polymerization of the benzoxazine precursors (resorcinol, formaldehyde, and DAH) and hydrolysis of TEOS, followed by pyrolysis and a silica-removal step. The use of TEOS and Pluronic F127 creates more porosity. Typically, resorcinol (0.5 g) and F127 (0.209 g) were dissolved in a mixed solvent of ethanol (2.25 g) and deionized water (1.5 g). TEOS (0.776 g) was then added under stirring to obtain a clear solution. Afterwards, DAH (0.026 g) was added to the above solution. Subsequently, a formalin solution (37 wt%) was injected into the solution to form a white homogeneous emulsion. This emulsion was then sealed and transferred into an oven at 90 °C. It quickly turned yellow and solidified to a gel within 15 min. This gel was cured for an additional 4 h under the same temperature. Finally, the as-made polymer monolith was dried at room temperature, followed by pyrolysis at 800 °C for 2 h under a nitrogen atmosphere, to obtain a porous carbon-silica hybrid. After removal of the silica with NaOH (4 M) solution, the porous carbons were obtained. By changing the amount of TEOS and the amount of ethanol and deionized water (Table 1), we can tune the mesopore/micropore volume ratio of the carbons. The carbon-

silica hybrids were denoted CSH-x and the obtained porous carbons were denoted PC-x, wherein x represents the silica content.

Electrochemical measurements

Electrochemical experiments were performed using CR2025 coin-type test cells assembled in an argon-filled glove box with lithium metal as the counter and reference electrodes at room temperature. For preparing the working electrode, an aqueous mixture of active material, conductive carbon black and LA133 (water-based binder, Indigo) at a weight ratio of 8:1:1 were pasted onto a rough Cu foil with a Celgard 2400 membrane as the separator to isolate electrons. The electrolyte was $LiPF_6$ (1 M) dissolved in a mixture of dimethyl carbonate (DMC), ethyl methyl carbonate (EMC) and ethylene carbonate (EC) (1:1:1 v/v/v) with fluorinated ethylene carbonate (FEC, 2 wt%) as an additive. The cells were assembled in an argon-filled glove-box. Galvanostatic charge-discharge cycles were tested by a LAND CT2001A electrochemical workstation at current densities of 100 mA g^{-1} to 3000 mA g^{-1} between 0.005 V and 3 V versus Li^+/Li at room temperature. Electrochemical impedance spectroscopy (EIS) measurements were carried out before charge-discharge cycles at a rate of 100 mA g^{-1} in the frequency range of 100 KHz to 0.01 Hz with a zero-bias potential and 5 mV amplitude.

Acknowledgements

The project was supported by the National Natural Science Funds for Distinguished Young Scholars (No.21225312) and the Special Program for Basic Research of the Ministry of Science and Technology (2012CB626802).

Keywords: carbon · electrochemical performance · energy conversion · lithium ion batteries · porous materials

[1] Y. G. Guo, J. S. Hu, L. J. Wan, *Adv. Mater.* **2008**, *20*, 2878 – 2887.
[2] M. Winter, R. J. Brodd, *Chem. Rev.* **2004**, *104*, 4245 – 4269.
[3] V. Etacheri, R. Marom, R. Elazari, G. Salitra, D. Aurbach, *Energy Environ. Sci.* **2011**, *4*, 3243 – 3262.
[4] S. R. Mukai, T. Hasegawa, M. Takagi, H. Tamon, *Carbon* **2004**, *42*, 837 – 842.
[5] T. Hasegawa, S. R. Mukai, Y. Shirato, H. Tamon, *Carbon* **2004**, *42*, 2573 – 2579.
[6] H. Nishihara, T. Kyotani, *Adv. Mater.* **2012**, *24*, 4473 – 4498.
[7] N. A. Kaskhedikar, J. Maier, *Adv. Mater.* **2009**, *21*, 2664 – 2680.
[8] J. M. Tarascon, M. Armand, *Nature* **2001**, *414*, 359 – 367.
[9] D. S. Su, R. Schlögl, *ChemSusChem* **2010**, *3*, 136 – 168.
[10] K. Tang, R. J. White, X. Mu, M-M. Titirici, P. A. van Aken, J. Maier, *ChemSusChem* **2012**, *5*, 400 – 403.
[11] B. K. Guo, X. Q. Wang, P. F. Fulvio, M. F. Chi, S. M. Mahurin, X. G. Sun, *Adv. Mater.* **2011**, *23*, 4661 – 4666.
[12] J. Sun, H. Liu, X. Chen, D. G. Evans, W. Yang, X. Duan, *Adv. Mater.* **2013**, *25*, 1125 – 1130.
[13] H. B. Li, W. J. Kang, Y. Yu, J. F. Liu, Y. T. Qian, *Carbon* **2012**, *50*, 4787 – 4793.
[14] S. Kawasaki, Y. Iwai, M. Hirose, *Carbon* **2009**, *47*, 1081 – 1086.
[15] R. Fernández-Saavedra, P. Aranda, E. Ruiz-Hitzky, *Adv. Funct. Mater.* **2004**, *14*, 77 – 82.
[16] S. H. Yoon, C. W. Park, H. Yang, Y. Korai, I. Mochida, R. T. K. Baker, *Carbon* **2004**, *42*, 21 – 32.
[17] F. D. Han, B. Yao, Y. J. Bai, *J. Phys. Chem. C* **2011**, *115*, 8923 – 8927.
[18] Y. S. Hu, P. Adelhelm, B. M. Smarsly, S. Hore, M. Antonietti, J. Maier, *Adv. Funct. Mater.* **2007**, *17*, 1873 – 1878.
[19] X. Zhao, C. M. Hayner, M. C. Kung, H. H. Kung, *ACS Nano* **2011**, *5*, 8739 – 8749.
[20] H. Zhou, S. Zhu, M. Hibino, I. Honma, M. Ichihara, *Adv. Mater.* **2003**, *15*, 2107 – 2111.
[21] G. P. Hao, F. Han, D. C. Guo, R. J. Fan, G. Xiong, W. C. Li, *J. Phys. Chem. A J. Phys. Chem. C.* **2012**, *116*, 10303 – 10311.
[22] Y. Chen, Z. Lu, L. Zhou, Y. W. Mai, H. Huang, *Energy Environ. Sci.* **2012**, *5*, 7898 – 7902.
[23] Y. Mao, H. Duan, B. Xu, L. Zhang, Y. Hu, C. Zhao, *Energy Environ. Sci.* **2012**, *5*, 7950 – 7955.
[24] M.-S. Kim, B. Fang, J. H. Kim, D. Yang, Y. K. Kim, T.-S. Bae, *J. Mater. Chem.* **2011**, *21*, 19362 – 19367.
[25] Y. Fang, Y. Lv, R. Che, H. Wu, X. Zhang, D. Gu, *J. Am. Chem. Soc.* **2013**, *135*, 1524 – 1530.
[26] J. R. Matos, M. Kruk, L. P. Mercuri, M. Jaroniec, L. Zhao, T. Kamiyama, *J. Am. Chem. Soc.* **2003**, *125*, 821 – 829.
[27] C. F. Xue, B. Tu, D. Y. Zhao, *Adv. Funct. Mater.* **2008**, *18*, 3914 – 3921.
[28] R. L. Liu, Y. F. Shi, Y. Wan, Y. Meng, F. Q. Zhang, D. Gu, *J. Am. Chem. Soc.* **2006**, *128*, 11652 – 11662.
[29] S. Pega, C. Boissiere, D. Grosso, T. Azais, A. Chaumonnot, C. Sanchez, *Angew. Chem. Int. Ed.* **2009**, *48*, 2784 – 2787; *Angew. Chem.* **2009**, *121*, 2822 – 2825.
[30] Y. Deng, T. Yu, Y. Wan, Y. Shi, Y. Meng, D. Gu, *J. Am. Chem. Soc.* **2007**, *129*, 1690 – 1697.
[31] A. H. Lu, F. Schuth, *Adv. Mater.* **2006**, *18*, 1793 – 1805.
[32] Y. Cao, L. Xiao, M. L. Sushko, W. Wang, B. Schwenzer, J. Xiao, *Nano. Lett.* **2012**, *12*, 3783 – 3787.
[33] J. L. Stevens, A. Y. Huang, H. Peng, I. W. Chiang, V. N. Khabashesku, J. L. Margrave, *Nano. Lett.* **2003**, *3*, 331 – 336.
[34] F. Anariba, U. Viswanathan, D. F. Bocian, R. L. McCreery, *Anal. Chem.* **2006**, *78*, 3104 – 3112.
[35] S. W. Lee, B. S. Kim, S. Chen, Y. Shao-Horn, P. T. Hammond, *J. Am. Chem. Soc.* **2009**, *131*, 671 – 679.
[36] S. Kundu, Y. Wang, W. Xia, M. Muhler, *J. Phys. Chem. C* **2008**, *112*, 16869 – 16878.
[37] X. C. Zhao, A. Q. Wang, J. W. Yan, G. Q. Sun, L. X. Sun, T. Zhang, *Chem. Mater.* **2010**, *22*, 5463 – 5473.
[38] H. R. Byon, B. M. Gallant, S. W. Lee, Y. Shao-Horn, *Adv. Funct. Mater.* **2013**, *23*, 1037 – 1045.
[39] U. Zielke, K. J. Hüttinger, W. P. Hoffman, *Carbon* **1996**, *34*, 983 – 998.
[40] F. D. Han, Y. J. Bai, R. Liu, B. Yao, Y. X. Qi, N. Lun, *Adv. Energy Mater.* **2011**, *1*, 798 – 801.
[41] S. Yang, X. Feng, L. Zhi, Q. Cao, J. Maier, K. Müllen, *Adv. Mater.* **2010**, *22*, 838 – 842.
[42] F. Han, D. Li, W. C. Li, C. Lei, Q. Sun, A. H. Lu, *Adv. Funct. Mater.* **2013**, *23*, 1692 – 1700.

Received: August 31, 2014
Published online on November 26, 2014